Research Article Adv. Mater. Lett. 2015, **6**(10), 924-929 Advanced Materials Letters

www.amlett.com, www.vbripress.com/aml, DOI: 10.5185/amlett.2015.6000 Published online by the VBRI Press in 2015

Thermal evolution of structural, optical and photocatalytic properties of TiO_2 nanostructures

Jaspal Singh, Satyabrata Mohapatra*

University School of Basic and Applied Sciences, Guru Gobind Singh Indraprastha University, Dwarka, New Delhi 110078, India

*Corresponding author. Tel: (+91) 11-25302414; E-mail: smiuac@gmail.com

Received: 22 May 2015, Revised: 23 July 2015 and Accepted: 28 July 2015

ABSTRACT

Nanostructures of TiO_2 were synthesized by a facile sol-gel method using pentanol as solvent. The effects of thermal annealing on the structural, optical and photocatalytic properties of as-synthesized TiO_2 nanostructures have been studied using X-ray diffraction (XRD), atomic force microscopy (AFM), Raman spectroscopy and UV-visible absorption spectroscopy. XRD and Raman spectroscopy results revealed that the synthesized TiO_2 nanostructures exist in anatase phase for annealing at temperatures up to 300 ^oC, while annealing at 600 ^oC led to the formation of TiO_2 nanostructures in anatase/rutile mixed-phase. AFM studies revealed the presence of TiO_2 nanorods, which showed a small decrease in aspect ratio upon annealing. The photocatalytic activity of nanostructured TiO_2 samples was evaluated through sun light driven degradation of methylene blue (MB) dye in water. TiO_2 nanorods in anatase/rutile mixed-phase in the sample annealed at 600 ^oC were found to exhibit the highest photocatalytic activity towards degradation of MB dye. The mechanism underlying the enhanced photocatalytic activity of TiO_2 nanostructures in anatase/rutile mixed-phase is tentatively proposed. Copyright © 2015 VBRI Press.

Keywords: TiO_2; nanostructures; photocatalysis; methylene blue.

Introduction

The path breaking discovery of photolysis of water on the surface of TiO_2 by Fujishima and Honda in 1972 [**1**] led to intensive research into the processes underlying photocatalytic water splitting [**2-4**] and paved the path for using solar energy by converting it into chemical/ electrical energy. Since then solar energy driven photochemical/ photocatalytic reactions and their practical applications have been of utmost interest and project great potential in environmental remediation and renewable energy applications [**5**]. TiO_2 is the most widely used metal oxide semiconductor photocatalyst owing to its high photocatalytic activity combined with its wide band gap, chemical stability, non-toxicity and low cost [**6**]. Nanostructured TiO_2 finds widespread applications in solar cells [**7**], CO_2 reduction [**8**], self-cleaning surfaces [**9**], electronics [**10**], as antibactericidal [**11**] and in environmental remediation [**12**]. Due to its strong redox activity TiO_2 exhibits highly enhanced photocatalytic activity leading to degradation of nearly all types of toxic organic pollutants.

TiO_2 exists in three polymorphs: anatase, rutile and brookite, amongst which the anatase and rutile phases (with band gaps of 3.20 and 3.03 eV, respectively) exhibit better photocatalytic activity [**13**]. The preferential nucleation of TiO_2 in anatase phase is attributed to its lower surface free energy as compared to the rutile phase, which explains the improved stability of anatase form at lower temperatures [**14**]. Upon annealing at high temperatures anatase and brookite TiO_2 transform into the rutile phase, which is the most stable polymorph of TiO_2. The photocatalytic activity of TiO_2 nanostructures is significantly influenced by parameters such as crystal structure, size, shape, surface area and surface morphology. Nakata *et al.* [**15**] reported that the crystal structure of TiO_2 significantly affects its photocatalytic activity. Generally, it is considered that the photocatalytic performance of TiO_2 in anatase phase is superior to that of rutile TiO_2 [**16, 17**]. It has been reported that the anatase/rutile mixed-phase TiO_2 exhibits higher photocatalytic activity as compared to the pure phases and the presence of a small fraction of rutile phase along with anatase TiO_2 leads to improved photocatalytic activity [**18, 19**]. Zhang *et al.* [**20**] reported the relationship between phase content and the photocatalytic properties of TiO_2 and demonstrated that the mixed phase can lead to improved photocatalytic activity. Xu *et al.* [**21**] synthesized mixed-phase TiO_2 nanocrystals with tunable brookite-to-rutile ratios and studied their photocatalytic activity towards degradation of Rhodamine B. They demonstrated that 100 mg of the photocatalyst degrades 5 mg/L RhB dye solution in 4 hours under irradiation with 500 W halogen tungsten lamp. Boehme *et al.* [**22**] demonstrated that anatase/rutile mixed phase TiO_2 nanotubes lead to photocatalytic degradation of 3.12×10^{-5} mol/L MB in 80 minutes under UV light. Therefore, controlling the phase constitution of nanostructured TiO_2 photocatalysts is very important for achieving highly enhanced photocatalytic activity. Several

 Copyright © 2015 VBRI Press

methods such as hydrothermal [**23**], solvothermal [**24**], chemical vapor deposition [**25**], sol-gel method [**26, 27**], ball milling [**28**], microemulsion [**29**] and sonochemical [**30**] methods have been used to synthesize TiO_2 nanostructures.

In this paper, we report facile synthesis of TiO_2 nanostructures in anatase/rutile mixed-phase by pentanol-assisted sol-gel method combined with thermal annealing. The effects of thermal annealing on the structural, optical and photocatalytic properties of the synthesized TiO_2 nanostructures have been investigated. We have demonstrated that TiO_2 nanorods with anatase/rutile mixed-phase exhibits highly enhanced photocatalytic activity towards sun light driven photocatalytic degradation of methylene blue (MB) dye in water. Though there are few studies reporting the photocatalytic activity of anatase/rutile mixed phase TiO_2 nanostructures, no one has achieved such highly enhanced photocatalytic activity which is very important for practical applications.

Experimental

Materials

Titanium (IV) tetraisopropoxide ($Ti[OCH(CH_3)_2]_4$) (TTIP) and 1-Pentanol ($C_5H_{12}O$) were used as the starting materials for the synthesis of TiO_2 nanostructures. Methylene blue (MB) was used as the model organic contaminant in water for evaluating the photocatalytic activity of synthesized nanomaterials. TTIP was purchased from Spectrochem, India while MB was purchased from SRL, India. 1-Pentanol was purchased from CDH, India. All the chemicals used were of analytical grade and were used as received without any further purification.

Synthesis of TiO_2 nanostructures

TiO_2 nanostructures were synthesized by pentanol-assisted sol-gel method at room temperature. In a typical synthesis, 0.3 M solution of TTIP in 40 mL 1-pentanol was prepared by mixing them under magnetic stirring. To control the hydrolysis rate and avoid any stabilizing agent, 20 mL solution of double distilled water and 1-pentanol mixed in 1:1 ratio was drop wise added into the solution under stirring. A yellowish transparent gel was formed after continuous stirring of the solution for 1 h. The gel was then recovered and thoroughly washed by repeated centrifugation-redispersion in 1-pentanol. The obtained gel was then dried at 80 °C over night. After drying the samples were annealed at 100 °C, 300 °C, 600 °C, and 900 °C for 4 h in air in a furnace. The powdered materials obtained after thorough grinding were used for characterizations and photocatalytic studies. The samples prepared upon annealing at different temperatures of 100 °C, 300 °C, 600 °C and 900 °C are hereafter referred to as T1, T3, T6 and T9, respectively.

Characterizations

The structural properties of the synthesized samples were determined using powder X-ray diffraction (XRD) (Panalytical X'pert Pro diffractometer; Cu K_α radiation λ = 0.1542 nm). Raman measurements were carried out using Horiba Jobin Vyon Raman spectrometer using excitation of 488 nm. The surface morphology of TiO_2 nanostructures was investigated by atomic force microscopy (AFM) using Park systems XE-70. The samples for AFM analysis were prepared by ultrasonically dispersing the powder samples in ethanol and drop coating the mixtures onto Si substrates.

The effects of thermal annealing on the photocatalytic activity of the synthesized nanostructured TiO_2 sample was evaluated by monitoring sun light driven degradation of methylene blue (MB) dye in water. Aqueous solution of MB of 7.9 μM concentration was prepared by dissolving MB in double distilled water. The concentration of MB in solution was determined by measuring the value at its characteristic wavelength of 664 nm using Hitachi U3300 dual beam spectrophotometer. The reaction suspensions were prepared by adding 2 mg of the samples T1, T3, T6 and T9 into 5 mL of the above mentioned MB solutions in glass vials. These suspensions were sonicated for 20 minutes and magnetically stirred for 30 minutes in dark to ensure an adsorption/desorption equilibrium. The reaction suspensions containing MB with or without photocatalyst samples T1, T3, T6 and T9 were irradiated with sun light for different durations of 6, 12, 18 and 24 minutes with intermittent shaking.

These suspensions were then centrifuged and the photocatalyst materials were removed from the suspensions. UV-visible absorption spectra of the solutions were recorded in the range of 200-800 nm, using a dual beam UV-visible spectrophotometer, with double distilled water as the reference medium. The photocatalytic efficiency of photocatalysts for photocatalytic degradation of MB was calculated using the following formula;

$$\eta = \frac{A_0 - A}{A_0} \qquad (1)$$

where, A_0 is the absorbance of MB dye in the solution without any photocatalyst before sun light exposure and A is the absorbance of MB in the solutions after exposure time *t*.

Results and discussion

Fig. 1(a) shows the XRD patterns of the synthesized nanostructured TiO_2 samples annealed at different temperatures of 100 °C, 300 °C, 600 °C and 900 °C. The observed strong peaks at 25.28° and 27.40° are characteristic peaks corresponding to anatase TiO_2 (101) and rutile TiO_2 (110), respectively [**31**]. The XRD patterns reveal six peaks marked (101), (103), (004), (112), (200) and (211) well indexed to anatase TiO_2 (JCPDS card No. 211272). The other six peaks marked (110), (200), (111), (210), (211) and (220) closely match with rutile TiO_2 (JCPDS card No.761940). The XRD spectra reveal that the samples T1 and T3 consists of TiO_2 nanostructures in anatase phase only, while the sample T6 consists of TiO_2 nanostructures in both anatase and rutile phases, whereas the sample T9 contains nanostructures of rutile TiO_2 only. The crystallite sizes of anatase and rutile phases were calculated using the Scherrer's equation,

$$t = \frac{0.94\lambda}{\beta Cos\theta} \qquad (2)$$

 Copyright © 2015 VBRI Press

where, θ is the diffraction angle, β is the full width at half maximum (FWHM) of the XRD peak, λ is the wavelength of the X-rays. The estimated average crystallite size for the synthesized TiO_2 samples increased from 33 to 52 nm as the annealing temperature is increased from 100 to 900 ^oC.

The phase content and crystalline sizes in the samples annealed at different temperatures are summarized in **Table 1**. The percentage of rutile phase (X_R) in the samples T6 and T9 are calculated using equation (3),

$$X_R = \frac{I_R}{0.884\ I_A + I_R}. \quad (3)$$

where, X_R is the weight fraction of the rutile phase, I_A is the diffraction peak intensity of the anatase (101) phase, and I_R is the diffraction peak intensity of the rutile (110) phase. The broad diffraction peaks in sample T1 are due to the presence of large fraction of atoms in the amorphous grain boundaries. The XRD spectrum for the sample T3 revealed peaks corresponding to anatase TiO_2 with a slight narrowing and small increase in the intensity of peaks, indicating increase in crystallinity of the sample. For the sample T6 annealed at 600 ^oC the presence of TiO_2 nanostructures in anatase-rutile mixed-phase with improved crystallinity has been observed. At this temperature 48% of anatase TiO_2 converted into the rutile phase. For the sample T9 prepared by annealing at 900 ^oC the anatase TiO_2 converted into the rutile phase and crystallinity of sample T9 has been significantly improved. The micro-strain in the TiO_2 nanostructures was analysed using the Williamson–Hall method [**32**]. The Williamson–Hall equation is given as,

$$\frac{\beta \mathrm{Cos}\,(\theta)}{\lambda} = \frac{1}{D_{hkl}} + \varepsilon_{hkl}\frac{\mathrm{Sin}\,(\theta)}{\lambda} \quad (4)$$

where, θ is the diffraction angle, β is the full width at half maxima (FWHM) of the XRD peak, λ is the wavelength of the X-rays, D_{hkl} is the effective crystallite size and ε_{hkl} is the micro- strain. Lattice strain has been calculated with the help of W-H plot of samples T1, T3, T6 and T9.

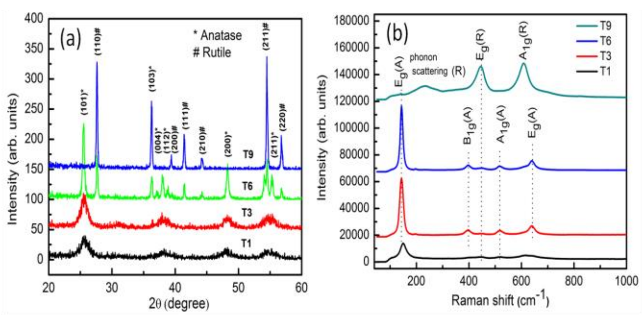

Fig. 1. (a) XRD patterns of nanostructured TiO_2 samples T1, T3, T6 and T9 and (b) Raman spectra of nanostructured TiO_2 samples T1, T3, T6 and T9.

The estimated lattice strain for the samples annealed at different temperatures is presented in **Table 1**. Sample T1 exhibits the highest lattice strain while sample T9 shows the lowest lattice strain. The highest lattice strain in sample T1 is due to the presence of an excess number of atoms and defects on the amorphous grain boundaries. The excess number of atoms and defects lead to lattice strain in the system [**33**]. Upon thermal annealing the crystallite size increases and defects gradually decrease, resulting in the relaxation of the lattice strain [**34**].

Table 1. Comparison of lattice strain, phase content and crystallite size of TiO_2 nanostructures in different samples.

Sample	Temperature (ºC)	Lattice strain	Phase content (%)	Crystalline size (nm)
T1	100	0.0252	A: 100	A: 6
T3	300	0.0238	A: 100	A: 7
T6	600	0.0056	A: 52, R: 48	A: 33, R: 44
T9	900	0.0035	R: 100	R: 52

Fig. 1(b) illustrates the Raman spectra of nanostructured TiO_2 samples annealed at temperatures varying from 100 to 900 ^oC. The Raman spectrum from sample T1 reveals broad peaks at 150 cm^{-1}, 398 cm^{-1}, 518 cm^{-1} and 648 cm^{-1}, which corresponds to the E_g, B_{1g}, A_{1g} and E_g modes of anatase TiO_2, respectively [**35**]. In addition to these modes a small peak at 444 cm^{-1} is also observed, which corresponds to the E_g mode of rutile TiO_2 [**36**]. The Raman spectra for the samples T3 and T6 showed similar peaks at 143 cm^{-1}, 395 cm^{-1}, 445 cm^{-1}, 517 cm^{-1}, and 639 cm^{-1}. The observed Raman peaks at 143 cm^{-1}, 517 cm^{-1}, and 639 cm^{-1} correspond to the B_{1g}, A_{1g} and E_g modes of anatase TiO_2, respectively, while the peak at 445 cm^{-1} comes from the E_g mode of rutile TiO_2 [**36, 37**]. It can be clearly seen that annealing at temperatures up to 600 ^oC resulted in significant enhancement in the intensity of the E_g mode of anatase TiO_2. Annealing at 900 ^oC (sample T9) resulted in a significant enhancement in the intensity of Raman peaks at 444 cm^{-1} and 607 cm^{-1} corresponding to the E_g and A_{1g} modes rutile TiO_2, whereas the modes corresponding to anatase TiO_2 drastically dimished in intensity, confirming almost complete phase conversion of anatase TiO_2 into rutile TiO_2. Sample T9 also shows a very broad peak at 233 cm^{-1}, which is due to phonon scattering [**38**]. The Raman results are consistent with our XRD results. The samples T1 and T3 contain pure anatase TiO_2, while the sample T6 consists of anatase/ rutile mixed-phase TiO_2 and the sample T9 is made up of pure rutile TiO_2. The values of the Raman shift and full width at half maximum (FWHM) of the peak corresponding to the E_g mode anatase TiO_2 are shown in **Table 2**.

Table 2. Comparison of Raman shift and FWHM of Raman peaks in different samples.

Sample	Raman shift (cm^{-1})	FWHM (cm^{-1})
T1	150	28.2
T3	143	16.6
T6	143	12.9
T9	141	9.6

It can be clearly seen that the FWHM showed a regular decrease with an increase in annealing temperature from 100 to 900 ^oC. As the size of nanostructures decreases, the phonons get increasingly confined within the nanostructures and the phonon momentum distribution increases. This

 Copyright © 2015 VBRI Press

leads to broadening of the momentum of the scattered phonon according to the law of conservation of momentum, causing a peak broadening as well as a shift of the Raman bands [**39**]. It has been known that the E_g peak is mainly caused by symmetric stretching vibration of O−Ti−O in TiO_2, the B_{1g} peak is caused by symmetric bending vibration of O− Ti−O, and the A_{1g} peak is caused by antisymmetric bending vibration of O−Ti−O [**40**].

Fig. 2(a-d) and **Fig. 3(a-d)** depict the two and three dimensional AFM images revealing the surface morphology of the samples T1, T3, T6 and T9, respectively. The surface morphological studies on all the samples revealed the presence of nanorod like structures. **Fig. 2(a)** shows the surface morphology of sample T1, which contains randomly distributed nanorod like structures. The average width and length of these nanorods have been estimated to be 40 nm and 72 nm, respectively. The AFM image of the sample T3 is shown in **Fig. 2(b)**, which does not show any appreciable change in surface morphology of nanostructured TiO_2 sample upon annealing at 300 ^oC apart from a small increase in the width and length of nanorods to 42 and 73 nm, respectively. **Fig. 2(c)** shows the surface morphology of sample T6. It can be clearly seen that the number density of nanorod like structures increased upon annealing at 600 ^oC. The average width and length of TiO_2 nanostructures in this sample increased to 44 nm and 79 nm, respectively. **Fig. 2(d)** shows the surface morphology of sample T9, which clearly show nanorods and their aggregates. Annealing at 900 ^oC resulted in slight increase in the width and length of nanorods to 49 nm and 85 nm, respectively. From the AFM images **Fig. 2** and **Fig. 3** it is clear that thermal annealing led to a change in the average size as the annealing temperature is increased from 100 to 900 ^oC. The line profiles across the length and width of one nanorod like structure marked by arrows in **Fig. 2(a)** are shown in **Fig. 2(e-f)**, which confirms the presence of nanorods in the sample.

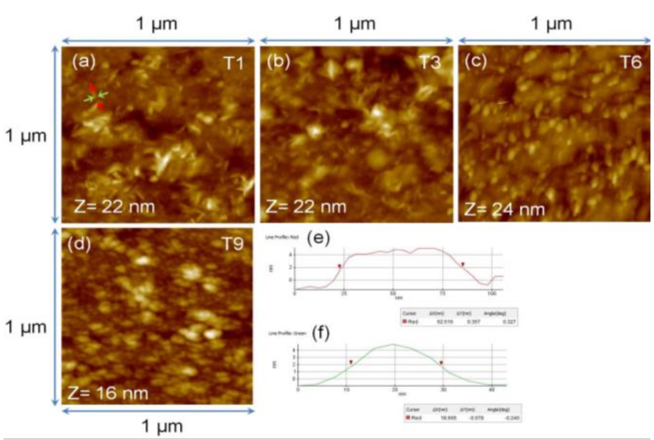

Fig. 2. (a-d) AFM images of TiO_2 nanostructures in the samples T1, T3, T6 and T9, (e-f) line profiles across length and width of one nanorod marked in (a).

The photocatalytic activity of the samples T1, T3, T6 and T9 towards sun light driven photocatalytic degradation of aqueous MB dye is monitored using UV-visible absorption spectroscopy. **Fig. 4(a-d)** shows the UV–visible absorption spectra of 7.9 μM MB aqueous solutions with 2mg of different photocatalysts T1,T3, T6 and T9 following sun light irradiation for different durations of time. It can be clearly seen that sample T6 with anatase/rutile mixed phase exhibits the highest photocatalytic efficiency as compared to the samples T1, T3 and T9. The photographs of glass vials, shown as insets in **Fig. 4(a-d)**, clearly show systematic changes in the color of MB with time. The glass vial appears colorless following 24 minutes of sunlight irradiation using T6 as photocatalyst (**Fig. 4(c)**). Our results clearly show that the photocatalytic activity is strongly dependent on the crystal structure and phase content of TiO_2 nanorods.

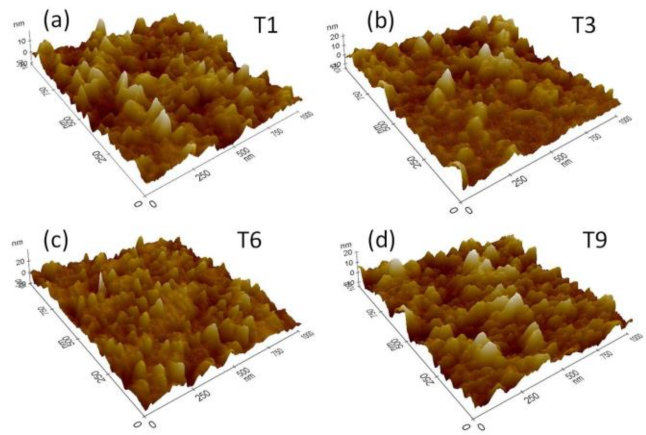

Fig. 3. (a-d) Three dimensional AFM images of TiO_2 nanostructures in the samples T1, T3, T6 and T9.

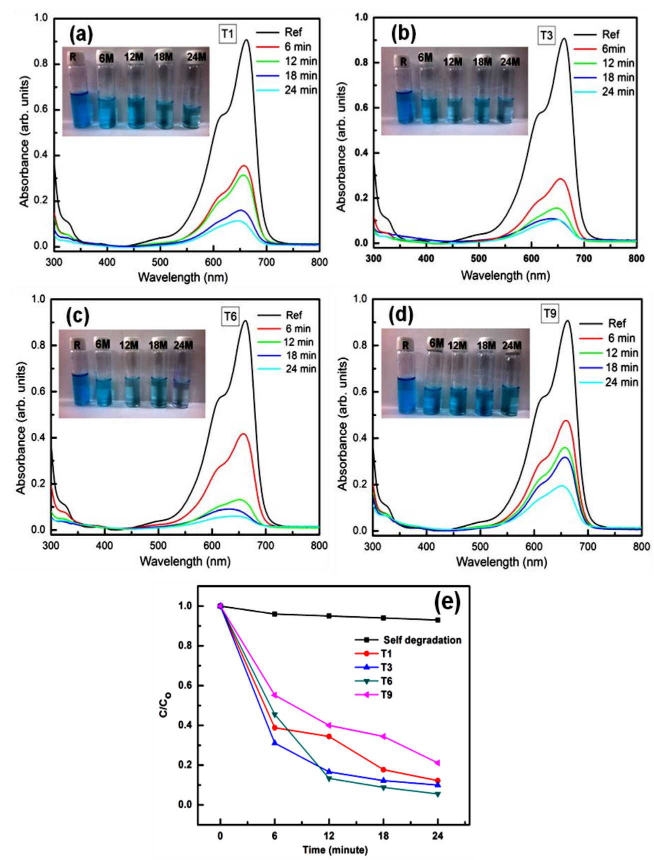

Fig. 4. (a-d) Optical absorption spectra showing temporal evolution of sun light driven photocatalytic degradation of MB in water using samples T1, T3, T6 and T9 as photocatalysts. (e) Kinetics of photocatalytic degradation of MB in water using samples T1, T3, T6 and T9 as photocatalysts.

Copyright © 2015 VBRI Press

Fig. 4(e) shows the kinetics of photocatalytic degradation of MB dye using samples T1, T3, T6 and T9 as photocatalysts. It can be seen that following 24 minutes of sun light exposure the samples T1, T3 and T9 led to degradation of 87%, 90% and 78% of MB dye, respectively whereas the sample T6 exhibited the highest photocatalytic efficiency of 94% for the same irradiation time. This clearly shows that anatase/rutile mixed-phase TiO_2 nanorods are more efficient photocatalysts as compared to the TiO_2 nanorods in pure anatase or rutile phase. In an earlier study, Mishra *et al.* [**41**] reported the photocatalytic activity of ZnO tetrapod like structures and showed that 60 mg of photocatalyst degrades 1µM of MB in 10 minutes under irradiation with UV light. Our results show much stronger activity of synthesized TiO_2 nanostructures towards degradation of 7.9 µM MB dye in water.

Fig. 5 shows the mechanism of photocatalytic activity of anatase/ rutile mixed-phase TiO_2 nanostructures. Anatase-rutile mixed phase TiO_2 has advantages over the single phase TiO_2 because of the improved separation of photogenerated charge carriers. The photogenerated electrons in the conduction band of rutile TiO_2 are captured by the anatase phase, which leads to improved charge separation and hence stronger photocatalytic activity [**42, 43**]. The photocatalytic degradation of MB dye using anatase/ rutile mixed-phase TiO_2 nanostructures can be understood as follows.

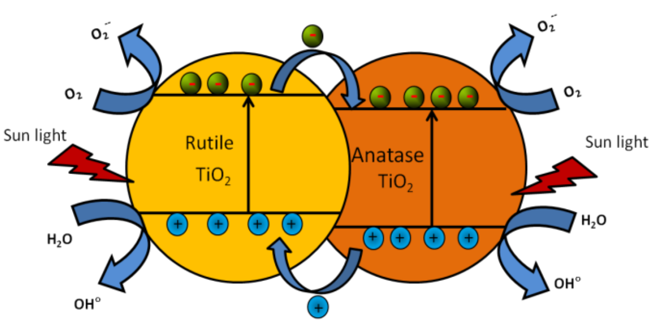

Fig. 5. Schematic diagram showing processes leading to sun light driven photocatalytic activity of TiO_2 nanostructures.

The first step involves adsorption of MB dye molecules onto the surface of TiO_2 nanostructures. Sun light irradiation leads to the generation of electron–hole (e^- - h^+) pairs in TiO_2 (eqn. 5). The photogenerated electrons in the conduction band of TiO_2 interact with the oxygen molecules adsorbed on TiO_2 to form superoxide radicals ($O_2^{\cdot}$) (eqn. 6). The holes generated in the valence band of TiO_2 react with water molecules to produce highly reactive hydroxyl radicals ($OH^{\cdot}$) (eqn.7). The highly reactive hydroxyl radicals ($OH^{\cdot}$) and superoxide radicals (O_2) react with MB dye molecule adsorbed on TiO_2 nanostructures and lead to its degradation resulting in its colourless form (eqn. 8 and eqn. 9). The processes underlying photocatalytic degradation of MB dye can be summarized by the following equations [11]

$$TiO_2 + h\nu \rightarrow e^- + h^+ \quad (5)$$
$$e^- + O_2 \rightarrow O_2^- \text{ (ad)} \quad (6)$$
$$h^+ + H_2O \rightarrow OH^{\cdot}\text{(ad)} + H^+ \quad (7)$$
$$OH^{\cdot} + \text{organic molecule} \rightarrow \text{degradation products} \quad (8)$$
$$O_2^- + \text{organic molecule} \rightarrow \text{degradation products} \quad (9)$$

Photocatalytic activity is strongly dependent on the morphology, crystallinity and the phase content of TiO_2 nanostructures. Our sample contains the TiO_2 nanorod-like structures which provide the higher surface area for adsorption of MB dye molecules. Wang *et al.* [**44**] synthesized pure rutile TiO_2 nanorods and studied the photocatalytic activity towards degradation of Rhodamine B in water under artificial solar light and showed that TiO_2 nanorods exhibit higher photocatalytic efficiency as compared to commercially available P25. Yu *et al.* [**45**] reported the synthesis of single-crystalline anatase TiO_2 nanorods by hydrothermal method and demonstrated that the nanorods show the higher photocatalytic activity for degrading organic pollutant. Baiju *et al.* [**46**] studied the effect of mixed-phase on the UV light driven photocatalytic activity of TiO_2. In our case, anatase/ rutile mixed-phase TiO_2 nanorods (sample T6) are found to exhibit highest photocatalytic efficiency as compared to pure anatase TiO_2 (samples T1 and T3) and pure rutile TiO_2 (sample T9) nanorods. The presence of anatase/ rutile mixed-phase TiO_2 nanorods in T6 leads to improved separation of charge carriers, leading to the marked enhancement in the photocatalytic activity.

Conclusion

In summary, TiO_2 nanorods were synthesized by pentanol-assisted facile sol-gel method. The effects of thermal annealing on the structural, optical and photocatalytic properties of TiO_2 nanorods in these samples were investigated. Nanostructured TiO_2 samples annealed at 600 ^{o}C exhibited highest photocatalytic activity towards sun light driven degradation of MB dye in water. The synthesized anatase/ rutile mixed-phase TiO_2 nanorods lead to improved separation of photogenerated charge carriers resulting in the observed highly enhanced photocatalytic activity.

Acknowledgements

The authors are thankful to Srikanth and Gurpreet for their help during XRD and Raman measurements, respectively. SM is thankful to Department of Science and Technology (DST), New Delhi for providing AFM and XRD facilities at Guru Gobind Singh Indraprastha University, New Delhi under Nano Mission program. JS is thankful to University Grants Commission (UGC), New Delhi for providing financial assistance through Maulana Azad National Fellowship.

Author contributions

Conceived the plan: SM; Performed the experiments: JS, SM; Data analysis: JS; Wrote the paper: JS, SM (JS, SM are the initials of authors). Authors have no competing financial interests.

Reference

1. Fujishima, A.; Honda, K.; *Nature* **1972**, *238*, 37-38.
   DOI: 10.1038/238037a0
2. Gratzel, M.; *Nature* **2001**, *414*, 338-344.
   DOI: 10.1038/35104607
3. Khan, S. U. M.; Al-Shahry, M.; Ingler, W. B.; *Science* **2002**, *297*, 2243-2245.
   DOI: 10.1126/science.1075035
4. Yang, H. G.; Sun, C. H.; Qiao, S. Z.; Zou, J.; Liu, G.; Smith, S. C.; Cheng, H. M.; Lu, G. Q.; *Nature* **2008**, *453*, 638-641.
   DOI: 10.1038/nature06964
5. Sang, L.; Zhao, Y.; Burda, C.; *Chem. Rev.* **2014**, *114*, 9283−9318.
   DOI: 10.1021/cr400629p
6. Schneider, J.; Matsuoka, M.; Takeuchi, Masato.; Zhang, J.; Horiuchi,Y.; Anpo, M.; Bahnemann, D. W.; *Chem. Rev.* **2014**, *114*, 9919−9986.

Copyright © 2015 VBRI Press

DOI: 10.1021/cr5001892
7. Oregan, B.; Gratzel, M.; *Nature* **1991**, *353*, 737 – 740. **DOI:** 10.1038/353737a0
8. Nguyen, T. V.; Wu, J. C. S.; Chiou, C. H.; *Catal. Commun.* **2008**, *9*, 2073–2076. **DOI:** 10.1016/j.catcom.2008.04.004
9. Quagliarini, E.; Bondioli, F.; Goffredo, G. B.; Cordoni, C.; Munafò, P.; *Constru. Build. Mater.* **2012**, *37*, 51–57. **DOI:** 10.1016/j.conbuildmat.2012.07.006
10. Wang, X.; Li, Z.; Shi, J.; Yu, Y.; *Chem. Rev.* **2014**, *114*, 9346−9384. **DOI:** 10.1021/cr400633s
11. Colmenares, J. C.; Luque, R.; Campelo, J. M.; Colmenares, F.; Karpiński, Z.; Romero, A. A.; *Materials* **2009**, *2*, 2228-2258. **DOI:** 10.3390/ma2042228
12. Hashimoto, K.; Irie, H.; Fujishima, A.; *Japan. J. Appl. Phys.* **2005**, *44*, 8269-8285. **DOI:** 10.1143/JJAP.44.8269
13. Yang, H. G.; Liu, G.; Qiao, S. Z.; Sun, C. H.; Jin, Y. G.; Zou, Z.; Smith, S. C.; Cheng, H. M.; Lu, G. Q.; *J. Am. Chem. Soc.* **2009**, *131*, 4078–4083. **DOI:** 10.1021/ja808790p
14. Zhao, L.; Liu, Y.; Wang, L.; Zhao, H.; Chen, D.; Zhong, B.; Wang, J.; Qi, T.; *Ind. Eng. Chem. Res.* **2014**, *53*, 70−77. **DOI:** 10.1021/ie4030598
15. Nakata, K.; Fujishima, A.; *J. Photochem. Photobiol. C* **2012**, *13*, 169–189. **DOI:** 10.1016/j.jphotochemrev.2012.06.001
16. Luttrell, T.; Halpegamage, S.; Tao, J.; Kramer, A.; Sutter, E.; and Batzill, M.; *Sci. Rep.* **2014**, *4*, 4043. **DOI:** 10.1038/srep04043
17. Lin, C. P.; Chen, H.; Nakaruk, A.; Koshy, P.; Sorrell, C. C.; *Energy Procedia* **2013**, *34*, 627-636. **DOI:** 10.1016/j.egypro.2013.06.794
18. Ju, M. G.; Sun, G.; Wang, J.; Meng, Q.; and Liang, W. Z.; *ACS Appl. Mater. Interfaces* **2014**, *6*, 12885−12892. **DOI:** 10.1021/am502830m
19. Liu, Z.; Zhang, X.; Nishimoto, S.; Jin, M.; Tryk, D. A.; Murakami, T., and Fujishima, A.; *Langmuir* **2007**, *23*, 10916-10919. **DOI:** 10.1021/la7018023
20. Zhang, J.; Xu, Q.; Feng,Z.; Li,M.; Li, C.; *Angew. Chem. Int. Ed.* **2008**, 47, 1766–1769. **DOI:** 10.1002/anie.200704788
21. Xu, H.; Zhang, L.; *J. Phys. Chem. C* **2009**, 113, 1785–1790. **DOI:** 10.1021/jp8089903
22. Boehme, M.; Ensinger, W.; *Nano-Micro Lett.* **2011**, 3, 236-241. **DOI:** 10.3786/nml.v3i4.p236-241
23. Nian, J. N.; Teng, H.; *J. Phys. Chem. B* **2006**, *110*, 4193–4198. **DOI:** 10.1021/jp0567321
24. Zhou, J.; Zhao, G.; Song, B.; and Han, G.; *CrystEngComm* **2011**, *13*, 2294-2302. **DOI:** 10.1039/C0CE00793E
25. Pazoki, M.; Taghavinia, N.; Abdi, Y.; Tajabadi, F.; Boschloo, G.; Hagfeldt, A.; *RSC* Adv. **2012**, *2*, 12278-12285. **DOI:** 10.1039/C2RA21361C
26. Lee, S.; Cho, I. S.; Lee, J. H.; Kim, D. H.; Kim, D. W.; Kim, J. Y.; Shin, H.; Lee, J. K.; Jung, H. S.; Park, N. G.; Kim, K.; Ko, M. J. and Hong, K. S.; *Chem. Mater.* **2010**, *22*, 1958–1965. **DOI:** 10.1021/cm902842k
27. Kumar, M.; Parashar, K. K.; Tandi, S. K.; Kumar, T.; Agarwal, D. C.; and Pathak, A.; *J. Spectroscopy*, **2013**, *2013*, Article ID 491716. **DOI:** 10.1155/2013/491716
28. Indris, S.; Amade, R.; Heitjans, P.; Finger, M.; Haeger, A.; Hesse, D.; Grunert, W.; Borger, A.; and Becker, K. D.; *J. Phys. Chem. B* **2005**, *109*, 23274-23278. **DOI:** 10.1021/jp054586t
29. Chhabra, V.; Pillai, V.; Mishra, B. K.; Morrone, A.; Shah, D. O.; *Langmuir* **1995**, *11*, 3307-3311. **DOI:** 10.1021/la00009a007
30. Zhu, Y.; Li, H.; Koltypin, Y.; Hacohen, Y. R.; and Gedanken, A.; *Chem. Commun.* **2001**, *24*, 2616-2617. **DOI:** 10.1039/B108968B
31. Zhang, Q.; Gao, L. and Guo, J.; *Appl. Catal. B* **2000**, *26*, 207–215. **DOI:** 10.1016/S0926-3373(00)00122-3
32. Parchur, A. K.; Ansari, A. A.; Singh, B. P.; Hasan, T. N.; Syed, N. A.; Raia, S. B. and Ningthoujam, R. S.; *Integr. Biol.* **2014**, *6*, 53. **DOI:** 10.1039/c3ib40148k
33. Choudhury B.; and Choudhury, A.; *Inter. Nano Lett.* **2013**, *3*, 55. **DOI:** 10.1186/2228-5326-3-55
34. Qin, W.; Szpunar, J. A.; *Phil. Mag. Lett.* **2005**, *85*, 649–656. **DOI:** 10.1080/09500830500474339
35. Chen, C. A.; Huang, Y. S.; Chung, W. H.; Tsai, D. S.; Tiong, K. K.; *J. Mater. Sci.* **2008**, *254*, 6915-6921. **DOI**: 10.1007/s10854-008-9595-3
36. Ohsaka, T.; Izumi, F.; Fujiki, Y.; *J. Raman Spectrosc.* **1978**, *7*, 321-324. **DOI**: 10.1002/jrs.1250070606
37. Porto, S. P. S.; Fleury, P. A.; Damen, T. C.; *Phys. Rev.* **1967**, *154*, 522-526. **DOI:** 10.1103/PhysRev.154.522
38. Shi, J.; Chen, J.; Feng, Z.; Chen, T.; Lian, Y.; Wang, X. and Li, C.; *J. Phys. Chem.C* **2007**, *111*, 693-699. **DOI:** 10.1021/jp065744z
39. Xu, C. Y.; Zhang P. X. and Yan, L.; *J. Raman Spectrosc.* **2001**, *32*, 862–865. **DOI:** 10.1002/jrs.773
40. Tian, F.; Zhang, Y.; Zhang, J. and Pan, C.; *J. Phys. Chem. C* **2012**, *116*, 7515−7519. **DOI:** 10.1021/jp301256h
41. Mishra, Y. K., Modi, G.; Cretu, V.; Postica, V.; Lupan, O.; Reimer, T.; Paulowicz, I.; Hrkac, V.; Benecke, W.; Kienle, L.; Adelung, R,; *ACS Appl. Mater. Interfaces* **2015**, 7, 14303−14316. **DOI:** 10.1021/acsami.5b02816
42. Nakajima, H.; Mori, T.; Shen, Q.; Taro, T. *Chem. Phys. Lett.* **2005**, *409*, 81-84. **DOI:** 10.1016/j.cplett.2005.04.093
43. Scanlon, D. O.; Dunnill, C. W.; Buckeridge, J.; Shevlin, S. A.; Logsdail, A. J.; Woodley, S. M.; Catlow, C. A.; Powell, M. J.; Palgrave, R. G.; Parkin, I. P.; Watson, G. W.; Keal, T. W.; Sherwood, P.; Walsh, A. and Sokol, A. A.; *Nature Mater.* **2013**, *12*, 798-801. **DOI:** 10.1038/NMAT3697
44. Wang, Y.; Zhang, L.; Deng, K.; Chen, X.; Zou, Z.; *J. Phys. Chem. C* **2007**, *111*, 2709-2714. **DOI:** 10.1021/jp066519k
45. Yu, Y.; Xu, D.; *Appl. Catal. B* **2007**, *73*, 166–171. **DOI:** 10.1016/j.apcatb.2006.07.017
46. Baiju, K. V.; Zachariah, A.; Shukla, S.; Biju, S.; Reddy, M. L. P.; Warrier, K. G. K.; *Catal. Lett.* **2009**, *130*, 130–136. **DOI:** 10.1007/s10562-008-9798-5

Advanced Materials Letters
Copyright © VBRI Press AB, Sweden
www.vbripress.com

JOURNAL VBRI Press
a rapid publication platform

Publish your article in this journal

Advanced Materials Letters is an official international journal of International Association of Advanced Materials (IAAM, www.iaamonline.org) published by VBRI Press AB, Sweden monthly. The journal is intended to provide top-quality peer-review articles in the fascinating field of materials science and technology particularly in the area of structure, sysnthesis and processing, characterisation, advanced-sate properties, and application of materials. All published articles are indexed in various databases and are available download for free. The manuscript management system is completely electronic and has fast and fair peer-review process. The journal includes review article, research article, notes, letter to editor and short communications.